

A Human-Robot Collaboration Framework for Improving Ergonomics During Dexterous Operation of Power Tools

Wansoo Kim^{a,1,*}, Luka Peternel^{b,1}, Marta Lorenzini^{a,c}, Jan Babič^d, and Arash Ajoudani^a

^aHRI² Lab, Department of Advanced Robotics, Istituto Italiano di Tecnologia, Genoa, Italy

^bDepartment of Cognitive Robotics, Delft University of Technology, Delft, The Netherlands

^cDepartment of Electronics, Information and Bioengineering, Politecnico di Milano, Milano, Italy

^dDepartment of Automation, Biocybernetics and Robotics, Jožef Stefan Institute, Ljubljana, Slovenia

Abstract

In this work, we present a novel control approach to human-robot collaboration that takes into account ergonomic aspects of the human co-worker during power tool operations. The method is primarily based on estimating and reducing the overloading torques in the human joints that are induced by the manipulated external load. The human overloading joint torques are estimated and monitored using a whole-body dynamic state model. The appropriate robot motion that brings the human into the suitable ergonomic working configuration is obtained by an optimisation method that minimises the overloading joint torques. The proposed optimisation process includes several constraints, such as the human arm muscular manipulability and safety of the collaborative task, to achieve a task-relevant optimised configuration. We validated the proposed method by a user study that involved a human-robot collaboration task, where the subjects operated a polishing machine on a part that was brought to them by the collaborative robot. A statistical analysis of ten subjects as an experimental evaluation of the proposed control framework is provided to demonstrate the potential of the proposed control framework in enabling ergonomic and task-optimised human-robot collaboration.

Keywords: Human-Robot Interaction, Ergonomics, Human performance modelling, Industrial/organizational/workplace safety

1. Introduction

The great potential and benefits of human-robot collaboration (HRC) are becoming increasingly evident in industrial communities that are influenced by a shift from mass production to highly customised, low volume manufacturing processes [1]. Collaborative robots can automatise repetitive and high-effort tasks and can reduce human task load by providing physical assistance, and therefore may potentially improve the working conditions of human workers. On the other hand, humans have better cognitive capability and can therefore supervise robots operation or transfer new skills to the collaborative robot [2, 3] thus adding a certain level of flexibility to the process and contributing to effective accomplishment of a broad range of manufacturing tasks.

One of the most evident problems that arises from the integration of the human co-worker into the robot's workspace is human safety. Ensuring a safe interaction between the human and robot counterparts should be the main prerequisite of any collaborative robot control. The prominent examples of such safety strategies are collision detection and reactive motion planning techniques [4, 5, 6], to avoid physical contacts between the robots and humans. Other approaches explore the use of compliance control strategies [7] to limit impact forces [8], or robots skins [9] to detect physical contacts and react accordingly. In this direction, a concept of safety map was recently introduced to give the controller the information about human injury occurrence and inherent global or task-dependent safety properties of a robot in a unified manner [10]. Furthermore, some researchers have proposed to use expert human demonstrations in an attempt to achieve safe collaborative behaviour of the robot [11, 12, 13, 3].

While the above mentioned strategies can prevent

*Corresponding author

Email address: wan-soo.kim@iit.it (Wansoo Kim)

¹These authors contributed equally to this work.

36 robots from causing physical injuries to human, never-
 37 theless, that does not mean the human will not sustain
 38 injuries that may come due to the improper task execu-
 39 tion or working conditions. In fact, former studies have
 40 shown that several occupational injuries and illnesses
 41 are caused by the exertion of excessive physical effort
 42 and repetitive motions in lifting, pushing or pulling on
 43 objects (e.g. drill, polish tool, etc.) [14, 15, 16]. In this
 44 direction, various heuristic, experienced-based guide-
 45 lines have been proposed to prevent injuries related to
 46 such work activities [17, 18], by focusing on human
 47 pose, tool or task types, and the environmental condi-
 48 tions. Nevertheless, most of the existing techniques to
 49 monitor human ergonomics neglect the dominant effect
 50 of interaction dynamics, which can contribute to the im-
 51 provement or worsening of human ergonomics, or they
 52 do not consider robotic co-workers [19].

53 To improve human ergonomics in interactive scenar-
 54 ios, the collaborative robots must observe and track
 55 human dynamic and kinematic states using their sens-
 56 sory systems (see Fig. 1). Nevertheless, the dynamical
 57 modelling of the human body is a very complex task
 58 [20, 21]. Such precise models may be computationally
 59 too expensive for on-line uses and are therefore limited
 60 to off-line processing [22, 16, 23]. Off-line techniques,
 61 on the other hand, lack the adaptability and may not be
 62 suitable in dynamically changing environments. Some
 63 previous work aimed at addressing the required on-line
 64 adaptability needs [24, 25, 26, 2, 27], however, only
 65 kinematic aspects of human partner were taken into ac-
 66 count. Other methods in HRC used on-line human ef-
 67 fort models that can approximate the dynamical aspects,
 68 such as minimum joint torque index [28] or muscle fat-
 69 igue index [3, 29], with the observation only limited to
 70 the human arm and did not consider human whole-body
 71 dynamics.

72 To address the above-mentioned limitations, we re-
 73 cently proposed a method for on-line estimation of the
 74 overloading joint torques² in static poses of the human
 75 body [30], which relies on a dynamic model of the hu-
 76 man and uses various real-time sensory measurements.
 77 The accuracy of the proposed model in estimation of
 78 the whole-body centre of pressure (CoP) and the over-
 79 loading joint torques has been evaluated in our previ-
 80 ous work [30]. A principled simplification of the human
 81 whole-body model enabled on-line estimation of human
 82 dynamic states. We then integrated this method into a
 83 robot control framework in HRC that enabled the robot
 84 to minimise the human overloading joint torques by as-

²The overloading joint torque refers to the torque induced into the human joint by an external load.

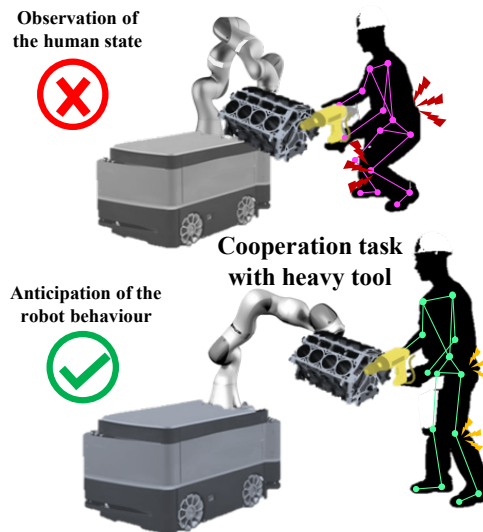


Figure 1: **The illustration of the proposed concept.** The proposed ergonomic control of human-robot collaboration aims to minimise the effect of overloading joint torques and maximise the arm manipulation ability while performing a repetitive manufacturing task.

85 sisting the human to work in a more suitable configu-
 86 ration [31]. Nevertheless, one of the disadvantages of
 87 this control framework was that it assumed static body
 88 pose of the human. More importantly, the method re-
 89 quired measurement of ground reaction forces of the
 90 human by force plates, which can severely reduce its
 91 applicability in realistic industrial settings. In addition,
 92 the method was not able to account for some impor-
 93 tant task-dependent parameters, such as manipulability
 94 of the human at hand, which can improve the effective-
 95 ness of collaboration and contribute to a better produc-
 96 tion quality.

97 The aim of this paper is to propose a novel human-
 98 robot collaboration control method that can guide hu-
 99 man co-workers to more ergonomic working configu-
 100 rations during dexterous operations such as drilling or
 101 polishing by using a power tool. Unlike the method in
 102 [31], the proposed method does not require the ground
 103 reaction force measurements during the on-line phase
 104 and is not limited to static poses³, both of which can
 105 increase its applicability in real industrial settings. Fur-
 106 thermore, the proposed method accounts for manipula-
 107 tion capacity of the human at hand during the optimisa-
 108 tion procedure, to ensure that the human has good ma-

³While in many industrial tasks the body remains relatively static during the task execution (e.g., polishing an object with a machine, etc.), many tasks involve some kind of arm movements that makes them dynamic.

manipulation capacity in the optimised configuration. We selected the two indicators so that one of them can account the dynamic aspects while the other can account for kinematic aspects, blending information about human dynamic loading and task performance which can contribute to reducing stress and improving productivity. Joint torque is a basic variable that describes the human effort, and reducing it would imply that the operator must provide less effort to perform a task. Meanwhile, manipulability can describe the controllability of the task velocities at hand, and can be associated with comfort since higher manipulability would simply imply easier control of the task velocities. However, there are other indicators that can be considered and selected for the optimisation. For additional indicator selection one can refer to the related literature [32, 33].

A user study which includes ten subjects provided detailed statistics in order to validate our approach. The experimental task was a collaborative polishing, in which the task of the human was to operate the polishing machine, while the appropriate robot motion that was to bring the object into the ergonomic working configuration. We analysed and compared the results of human overloading joint torques in the body, human arm manipulability capacity, and measured muscle activities in the arm between six pre-selected working configurations, spread across the human arm workspace, and the optimised configuration, as obtained by the proposed method.

A preliminary study of this work was presented at 2017 IEEE-RAS International Conference on Humanoid Robotics [34]. The specific contributions of this paper that go beyond the preliminary study are: 1) considerable extension of method formulation that takes into account human muscular manipulability instead of a classic manipulability, which does not properly account for human biomechanics, 2) experiments on ten subjects supported with statistical analysis and 3) a thorough evaluation procedure.

2. Observation layer

In this section, we introduce an observation layer to monitor the human current states in real-time. This layer measures the human kinematics and uses a dynamic model of the human to estimate the overloading joint torques in the body. We first need to perform an off-line calibration to identify the subject-dependent parameters of the dynamical model, it will be explained in the human whole-body model by using the statically equivalent serial chain (SESC) technique. Once the pa-

rameters are identified, the model is used for the real-time estimation of human overloading joint torques.

2.1. Human Whole-Body Model

The proposed estimation of human overloading joint torques is based on the method we recently proposed in [31]. In this approach, the overloading joint torques are determined by the difference of CoP displacement and the ground reaction forces (GRF) relation between the condition where the effect of an external interaction force is present and where it is not present. However, one of the limitations of this approach is that it assumes a static condition of the human body. Another limitation is that it needs an external force plate to measure the CoP that is affected by the interaction force. In this paper, we extend the previous concept in order to make the estimation of the overloading joint torque in dynamic poses without using external force plate devices.

The CoP components in the dynamic condition are characterised by the differences between the acceleration about the centre of mass (CoM) and the angular momentum [35, 36]. Let $\mathbf{C}_P = [C_{Px} \ C_{Py}]^T \in \mathbb{R}^2$ and $\mathbf{C}_M = [C_{Mx} \ C_{My} \ C_{Mz}]^T \in \mathbb{R}^3$ denote CoP and CoM, respectively. Let us suppose we have a whole-body modelled by a point mass, and such a model, resting on a flat ground and rotationally stable, the rate of change of spin angular momentum is equivalent to zero. Thus, \mathbf{C}_P can be represented as

$$\mathbf{C}_P = \begin{bmatrix} C_{Px} \\ C_{Py} \end{bmatrix} = \begin{bmatrix} C_{Mx} \\ C_{My} \end{bmatrix} - \frac{(C_{Mz} - C_{Pz})}{\dot{C}_{Mz} + g_z} \begin{bmatrix} \dot{C}_{Mx} \\ \dot{C}_{My} \end{bmatrix}, \quad (1)$$

where g_z is acceleration due to gravity, and C_{Pz} is the height of ground, which is equal to zero, since we assume that the ground is flat and is not moving with respect to Σ_W . As such, the CoP vector can be obtained by taking the CoM. We use a SESC technique [37] in order to determine the whole-body CoM of an articulated multi-body system (e.g. human). The CoM of a model with an n number of links as

$$\mathbf{C}_M = \mathbf{x}_0 + \mathbf{B}\Phi, \quad (2)$$

where $\mathbf{x}_0 \in \mathbb{R}^3$ is the position of the human floating base frame Σ_0 , which is connected to the inertial frame Σ_W .

To identify the subject parameters $\hat{\Phi}$, a linear system in (2) should be solved by a classical least-squares problem. To do this, measuring two components (i.e., x and y) of the \mathbf{B} and ${}^0\mathbf{C}_M = \mathbf{C}_M - \mathbf{x}_0$ for p poses should be taken. Although not all CoM information but two components as ${}^0C_{Mx,y}$ are measured by the measurement (e.g. force plate, etc.), we are able to create a linear system when an enough set of p poses are measured.

Let $\mathbf{\Omega} = [{}^0C_{1|M_x} \quad {}^0C_{1|M_y} \quad \dots \quad {}^0C_{p|M_x} \quad {}^0C_{p|M_y}]^T$ be a $2p \times 1$ vector that is composed of the stack of measured CoM's x and y component. Similarly, the stacked orientation matrix \mathbf{W} due to the p poses can be constructed a $2p \times 3(n+1)$ matrix by using the rows of the orientation matrix \mathbf{B} . The stacked matrix \mathbf{W} is invertible by using Moore-Penrose generalised inverse as $\mathbf{W}^+ = (\mathbf{W}^T \mathbf{W})^{-1} \mathbf{W}^T$, we then identify the SESC parameters vector $\hat{\mathbf{\Phi}}$ as (details can be found in [31])

$$\hat{\mathbf{\Phi}} = \mathbf{W}^+ \mathbf{\Omega}. \quad (3)$$

As a consequence, we can obtain a real-time estimation of CoP vector $\hat{\mathbf{C}}_p \in \mathbb{R}^2$ from (1) using an on-line estimation of the human CoM $\hat{\mathbf{C}}_M$, as well as its acceleration. The estimated subject-specific SESC parameters during an off-line calibration phase in (3) are used in (2) to obtain the on-line CoM model. The acceleration of the CoM vector is then calculated by using the Kalman filtering approach [38].

The basic strategy of the previous approach to estimate the overloading joint torques is to use the model-estimated whole-body CoP $\hat{\mathbf{C}}_{P_{wo}}$ and the measured CoP $\mathbf{C}_{P_{wt}}$ in conditions with or without the effect of external forces [31]. However, in this case, external sensory devices (e.g., force plate, sensor insoles) are required which would hinder the applicability. An extension of this approach considers to increase the applicability in realistic scenarios (e.g., industrial setting) that eliminates the requirement of using extra sensory systems.

In this paper, we propose an extension of SESC parameters that addresses the presence of an external object/tool (e.g., tool, machine, etc.) that is being manipulated by the human. The contribution of this extension can update the human CoP model to include an external object/tool, it is able to obtain the CoP in real-time instead of measuring it. Such an approach can be applied in cases when the robot can either estimate the parameters of unknown object/tool (e.g., measurement by its own sensory system as the force/torque sensor, torque sensor, etc.), when objects/tools are estimated by the perception system according to the predefined tool database (e.g., detect by the vision system, etc.).

The modified SESC parameters refer to the new mass distribution of a branch where the external object/tool is manipulated. Let $\bar{\mathbf{\Phi}} = [\bar{\boldsymbol{\phi}}_0^T \quad \dots \quad \bar{\boldsymbol{\phi}}_n^T]^T$ be a $3(n+1) \times 1$ vector of the modified SESC parameters. When the object/tool is applied to the end-point of a branch (e.g., hand, foot, etc.), the k -th modified SESC parameter, where k refers to an index of a segment within the

branch (e.g., base, upper arm, and lower arm), should be updated as

$$\bar{\boldsymbol{\phi}}_k = \frac{1}{M + m_e} (M \boldsymbol{\phi}_k + m_e^k \mathbf{d}_{k|next}), \quad (4)$$

where M is the total mass represented by the sum of the whole-body link masses and m_e is the external object/tool mass. ${}^k \mathbf{d}_{k|next} \in \mathbb{R}^3$ is the link length vector of the k -th segment measured from the frame attached to k -th segment to the next segment in the engaged branch. Intuitively, the last segment of the modified SESC model can be considered by an extension of the original SESC to the additional segment as the external object/tool. Hence, the link length of the last k -th segment is obtained by CoM of the external object/tool. For example, if the the object/tool is applied to the right hand (i.e, the segment's index of right arm branch is $k \in [0, 3, 4]$), the SESC parameters of right arm will be achieved by the link length; ${}^0 \mathbf{d}_{0|next}$: base to right shoulder; ${}^3 \mathbf{d}_{3|next}$: right shoulder to right elbow; ${}^4 \mathbf{d}_{4|next}$: right elbow to CoM position of the external object/tool.

Using the real-time CoP estimation function (1), the CoP with externally loaded condition $\hat{\mathbf{C}}_{P_{wt}}$ is calculated by using the extended model $\bar{\mathbf{\Phi}}$ from (4) in (2).

2.2. The Overloading Joint Torque

In the proposed method, the floating base human model is used in a way that each link of human is articulated through n revolute joints, whose locations are defined by a local reference frame Σ_i at the corresponding joint. The pelvis link is selected as a base frame Σ_0 . The system configuration is represented as $\mathbf{q} = [\mathbf{x}_0^T \quad \boldsymbol{\theta}_0^T \quad \mathbf{q}_h^T]^T \in \mathbb{R}^{6+n}$, where $\mathbf{x}_0 \in \mathbb{R}^3$ and $\boldsymbol{\theta}_0 \in \mathbb{R}^3$ are the position and orientation of Σ_0 with respect to Σ_w , while \mathbf{q}_h are angular positions of n human joints. The spatial velocity of the base frame can be expressed as $\boldsymbol{\vartheta}_0 = [\mathbf{v}_0^T \quad \boldsymbol{\omega}_0^T]^T \in \mathbb{R}^6$, where \mathbf{v}_0 and $\boldsymbol{\omega}_0$ correspond to linear and angular velocities, respectively.

The dynamic relationship between the body motion and external forces at various contact points is given as

$$\mathbf{M} \begin{bmatrix} \dot{\boldsymbol{\vartheta}}_0 \\ \dot{\mathbf{q}}_h \end{bmatrix} + \mathbf{C} \begin{bmatrix} \boldsymbol{\vartheta}_0 \\ \mathbf{q}_h \end{bmatrix} + \mathbf{G} = \mathbf{S}^T \boldsymbol{\Gamma} + \sum_{i=1}^{n_k} \mathbf{J}_{p_i}^T \mathbf{F}_i, \quad (5)$$

where \mathbf{M} , \mathbf{C} , and \mathbf{G} represent the inertia matrix, vector of centrifugal and Coriolis forces, and vector of the gravity force, respectively. $\mathbf{S} = [\mathbf{0}_{n \times 6} \quad \mathbf{I}_{n \times n}]$ is a selection matrix for the actuated joints and $\boldsymbol{\Gamma}$ is the $n \times 1$ vector of applied joint torques. \mathbf{J}_{p_i} is the Jacobian of

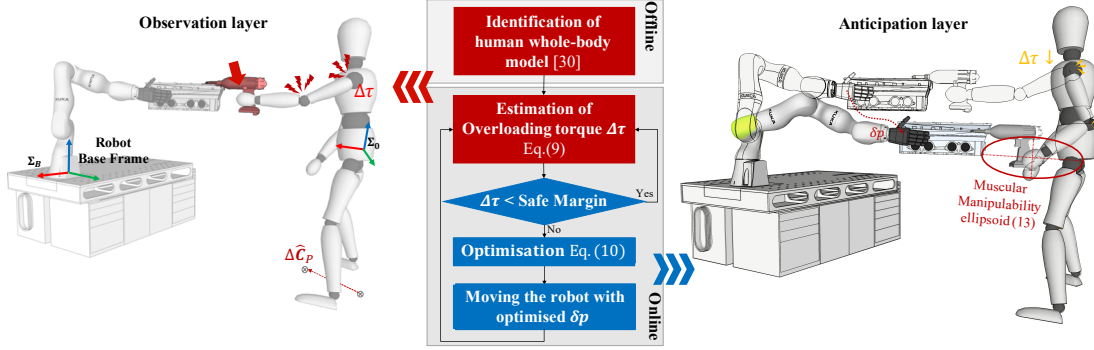


Figure 2: **The overall procedure of the proposed method.** The observation (left) and the anticipation layer (right) for estimating and reducing the overloading joint torques in human-robot collaboration are illustrated.

291 the contact constraints \mathbf{p}_i , where the n_k number of con- 319
 292 straint contact wrenches \mathbf{F}_i are applied with respect to 320
 293 Σ_W . Such a Jacobian matrix $\mathbf{J}_{p_i} = [\mathbf{J}_{p_i}^b \quad \mathbf{J}_{p_i}^r]$ reveals 321
 294 the contribution from the passive chain for the floating 322
 295 base and the actuate joints on the branch where $\mathbf{J}_{p_i}^r$ cor- 323
 296 responding to the displacement of joints on the contact 324
 297 point with respect to the base frame Σ_0 .

298 The overloading joint torques are calculated from the 325
 299 difference between the joint torques calculated in condi- 326
 300 tions with and without the external forces. Due to 327
 301 the external load, the CoP is also displaced compared 328
 302 to the CoP in the unloaded condition. Similarly to (5), 329
 303 the torque vector in condition without the external force 330
 304 Γ_{wo} is expressed by using estimated whole-body CoP 331
 305 $\hat{\mathbf{C}}_{P_{wo}}$ from the original SESC parameters in (3) as

$$306 \quad \mathbf{S}^T \Gamma_{wo} = \Gamma_b - \sum_{i=1}^{n_f} \mathbf{J}_{\hat{\mathbf{C}}_{P_{wo}i}}^T \mathbf{F}_{i|wo}, \quad (6)$$

307 where $\Gamma_b \in \mathbb{R}^{n+6}$ corresponds to the left part of (5), 332
 308 which is the joint torque vector of human body without 333
 309 the contact constraints (e.g., ground contact, hand con- 334
 310 tact, etc.). $n_f \in [1, 2]$ is the number of ground contact 335
 311 points at the foot. The vertical GRF (vGRF) \mathbf{F}_{wo} , which 336
 312 is obtained from the human body mass, act on the hu- 337
 313 man body by the transpose of the Jacobian as $\mathbf{J}_{\hat{\mathbf{C}}_{P_{wo}i}}^T \mathbf{F}_{i|wo}$

314 at the point of estimated CoP $\hat{\mathbf{C}}_{P_{wo}i}$. 338
 315 On the other hand, the condition with the external ob- 339
 316 ject/tool produces a torque Γ_{wt} , which is calculated by 340
 using $\hat{\mathbf{C}}_{P_{wt}}$ from the modified SESC parameters as

$$317 \quad \mathbf{S}^T \Gamma_{wt} = \Gamma_b - \sum_{i=1}^{n_f} \mathbf{J}_{\hat{\mathbf{C}}_{P_{wt}i}}^T \mathbf{F}_{i|wt} - \sum_{j=1}^{n_h} \mathbf{J}_{a_{hj}}^T \mathbf{F}_{j|h}, \quad (7)$$

318 where \mathbf{F}_{wt} is the vGRF vector applied at $\hat{\mathbf{C}}_{P_{wt}}$ in this 341
 condition that is obtained from the combined mass of

the human body and the external object/tool. \mathbf{F}_h repre- 320
 sents the pre-estimated mass of the object/tool that are 321
 applied at the contact points \mathbf{a}_h . $\mathbf{J}_{\hat{\mathbf{C}}_{P_{wt}i}}$ and $\mathbf{J}_{a_{hj}}$ refer to 322
 the contact Jacobian at the point of $\hat{\mathbf{C}}_{P_{wt}i}$ and \mathbf{a}_{hj} , re- 323
 spectively. $n_h \in [1, 2]$ is the number of operated hands 324
 where the tools/objects are handled.

Consequently, the overloading joint torques are defined 325
 by the difference between the torque vectors from 326
 (6) and (7) as

$$327 \quad \mathbf{S}^T \Delta \Gamma = \sum_{j=1}^{n_h} \mathbf{J}_{a_{hj}}^T \eta_j \Delta \mathbf{F} - \sum_{i=1}^{n_f} \left(\mathbf{J}_{\hat{\mathbf{C}}_{P_{wt}i}}^T - \mathbf{J}_{\hat{\mathbf{C}}_{P_{wo}i}}^T \right) \mathbf{F}_{i|wt} 328 \\ + \mathbf{J}_{\hat{\mathbf{C}}_{P_{wo}i}}^T \zeta_i \Delta \mathbf{F}, \quad (8)$$

329 where $\Delta \mathbf{F} = \sum_{i=1}^{n_f} \Delta \mathbf{F}_{i|w} = -\sum_{j=1}^{n_h} \mathbf{F}_{j|h}$ is the sum of 330
 the interaction forces. As regards the distribution gain 331
 ($\sum_i \zeta_i = 1$ and $\sum_j \eta_j = 1$) related to the number of con- 332
 tact points, we can consider that the gain is defined by 333
 the employed human model; for example, if the model 334
 is interacting with environment using a single arm and 335
 single foot, hence $\eta = 1$ and $\zeta = 1$. A further exam- 336
 ple of the multi-interaction model has been reported in 337
 [39] where the model assumes a symmetric distribution 338
 of the grasp forces in two hands while carrying an ob- 339
 ject ($\eta_j = 0.5$), but the force distribution on the feet (ζ_i) 340
 is computing by the synergistic model approach in real- 341
 time.

3. Anticipation layer

This section introduces an anticipation layer⁴ that is 342
 used by the robot to predict the optimal configuration

⁴The "anticipation" refers to the ability of the method to anticipate 343
 overloading joint torques and then react to minimise them. 344

341 of task execution to accommodate ergonomic working
 342 conditions for the human co-worker. This layer relies
 343 on the observation layer (see Fig. 2) to obtain the de-
 344 sired configuration of the task execution through a con-
 345 strained optimisation technique that reduces the joint
 346 torque variation of human under several constraints. In
 347 particular, we used the human arm muscular manipu-
 348 lability as a constraint in this optimisation to facilitate
 349 the human movements in achieving a good manipula-
 350 tion capacity in the optimised configuration.

3.1. Optimisation

351 Here we present the minimisation procedure of hu-
 352 man overloading joint torque vector with respect to
 353 body configuration and given constraints. This consid-
 354 eration was to avoid potential injuries caused by the ex-
 355 cessive loading effect during the execution of a collabo-
 356 rative task.
 357

The optimisation process is defined as

$$\min_{\mathbf{q}_h} \|\Delta\mathbf{\Gamma}^T \mathbb{W} \Delta\mathbf{\Gamma}\|, \quad (9)$$

359 where $\Delta\mathbf{\Gamma} \in \mathbb{R}^n$ is the overloading joint torques
 360 vector which is obtained from (8) and $\mathbb{W} =$
 361 $\text{diag}[\Delta\mathbf{\Gamma}_1/\mathbf{\Gamma}_{\max_1} \cdots \Delta\mathbf{\Gamma}_n/\mathbf{\Gamma}_{\max_n}] \in \mathbb{R}^{n \times n}$ is the
 362 weight matrix with components $\mathbf{\Gamma}_{\max_n}$. Although the
 363 maximum joint torque values are not explicitly reported
 364 in previous works, however, starting from the torque ca-
 365 pacity values of the work by Snook and Ciriello [40]
 366 such weighing factor can be tuned experimentally.

367 In the optimisation process, we consider several con-
 368 straints. To ensure a safe configuration after the opti-
 369 misation, upper and lower bounds \mathbf{q}_L and \mathbf{q}_U of the human
 370 joint angles are constrained within the human body lim-
 371 itations. The postural stability in an arbitrary configu-
 372 ration is considered by position of the CoP $\mathbf{C}_P \in \mathbb{R}^2$,
 373 which should only exist inside the stable region \mathcal{E}_s (i.e.
 374 within the support polygon of feet). The robot end-
 375 effector position that controls the placement of the co-
 376 manipulated object is constrained within the feasible
 377 shared workspace of the human and the robot. The ap-
 378 plication of such constraints in the optimisation process
 379 ensures the stability and safety of the human co-worker
 380 and the collaboration task.

381 The final constraint is the endpoint manipulability of
 382 the human arm. In general, humans adjust the con-
 383 figuration of their body and limbs in order to max-
 384 imise the kinematic and dynamic properties according
 385 to given tasks and environmental conditions [41]. In
 386 robotics, the classic measure for the kinematic and dy-
 387 namic properties of a robot end-effector is the *manip-*
 388 *ulability*, which provides an idea of how well the end-

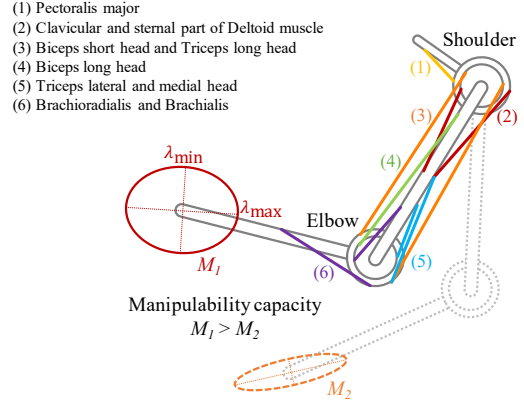


Figure 3: **Ten muscles are considered in the definition of arm manipulability capacity.** The resulting ellipsoid and its major and minor axes are conceptually illustrated in this figure.

389 effector can produce velocity or force in different direc-
 390 tions of the Cartesian space [42]. Manipulability can
 391 be geometrically represented as an ellipsoid at the end-
 392 effector, whose radius in a specific direction indicates
 393 the velocity/force production ability. In a specific ex-
 394 ample, if the task requires that the object/tool is manip-
 395 ulated in a complex manner, which involves production
 396 of end-effector force and velocity equally in various di-
 397 rections of Cartesian space, the configuration of the arm
 398 should be maintained close to where endpoint manipu-
 399 lability ellipsoid is isotropic. Nevertheless, the classic
 400 manipulability, which has been extensively studied in
 401 the robotic manipulators actuated by electric motors, is
 402 not able to faithfully measure the manipulation ability
 403 of the human body. This is because the human body is
 404 actuated by the muscles that have spring-like properties
 405 and antagonistically pull the joint in different directions.
 406 Therefore, it is necessary to account for the effect of this
 407 specific feature of human actuators on the endpoint ma-
 408 nipulability. To do so, we include *muscular manipula-*
 409 *bility* [43, 44] in the proposed optimisation process as a
 410 constraint condition. Hence, in our work, the position of
 411 the object/tool being co-manipulated is also constrained
 412 by the human arm muscular manipulability.

The relation between the muscle forces and the end-
 413 point force is defined as

$$\mathbf{F} = \mathbf{J}_a^{+T} \mathbf{J}_m^T \mathbf{F}_m, \quad (10)$$

415 where \mathbf{F} is endpoint force, which can be one of the ex-
 416 ternal contact wrenches from (5), \mathbf{J}_a^+ is MoorePenrose
 417 inverse of the geometric Jacobian matrix of arm, \mathbf{J}_m is
 418 muscle Jacobian matrix that contains muscle moment
 419 arms at the joints, and \mathbf{F}_m is muscle force, which we

420 calculate by using the Hill’s muscle model

$$\mathbf{F}_m = \mathbf{F}_{hill}\alpha, \quad (11)$$

421 where $0 \leq \alpha \leq 1$ muscle activation and \mathbf{F}_{hill} is a diago-
422 nal matrix representing the Hill’s muscle force.

423 By combining (10) and (11), the muscular manip-
424 ulability is obtained from expression $(\mathbf{J}_a^{+T} \mathbf{J}_m \mathbf{F}_{hill})$ that
425 transforms muscle activations to Cartesian endpoint
426 force. Unlike classic manipulability measure that con-
427 sideres only geometric Jacobian \mathbf{J}_a , muscular manipula-
428 bility takes into account also muscle Jacobian \mathbf{J}_m . As-
429 suming $\|\alpha\| < 1$, we can derive the expression to obtain
430 the manipulability (see [44] for details)

$$\mathbf{K} = (\mathbf{J}_a^{+T} \mathbf{J}_m \mathbf{F}_{hill})(\mathbf{J}_a^{+T} \mathbf{J}_m \mathbf{F}_{hill})^T. \quad (12)$$

431 By applying singular value decomposition of \mathbf{K} we ob-
432 tained the eigenvalues λ that represent the axial lengths
433 of the endpoint manipulability ellipsoid. Consequently,
434 the manipulability capacity $M = \frac{\lambda_{\min}}{\lambda_{\max}}$ was defined as a
435 ratio between the minimum and the maximum eigen-
436 value. For our experiments we normalised this value to
437 the maximum ratio of the entire workspace, which gave
438 us a percentage value. A higher value of manipulability
439 capacity indicates that the capacity to produce the arm
440 endpoint force and velocity is better in all directions of
441 the Cartesian space.

442 Our arm model included two segments and two joints
443 (3 DoF in the shoulder and 1 DoF in the elbow). We
444 considered ten muscles (see Fig. 3): clavicular and ster-
445 nal part of Deltoid muscle (shoulder), Pectoralis ma-
446 jor (shoulder), Biceps short head and Triceps long head
447 (bi-articular), Biceps long head (elbow), Triceps lateral
448 and medial head (elbow), Brachioradialis (elbow) and
449 Brachialis (elbow).

450 To ensure good manipulability in all directions of hu-
451 man arm endpoint, we defined a certain degree of man-
452 ipulability capacity as an optimisation constraint. The
453 method therefore searched for the optimal minimum
454 overloading joint torques within configurations, where
455 the manipulability ellipsoid was close to isotropic. The
456 optimisation problem of (9) was used to formulate
457 a nonlinear programming problem, which was then
458 solved using the active set method of the ALGLIB opti-
459 misation library.

460 3.2. Execution of the robot behaviour

461 To achieve a more ergonomic working condition of
462 the human co-worker, the robot uses the optimised con-
463 figuration of the human body obtained through (9). Us-
464 ing the forward kinematics, the current human configu-
465 ration and the optimised one are expressed in Cartesian

466 space. The difference between the two is used to calcu-
467 late the robot end-effector trajectory, which brings the
468 human from the current to the optimised configuration.

469 To achieve safe and adaptive interaction between the
470 human and robot, the Cartesian impedance controller by
471 default was set the stiffness parameter to 1500 N/m in
472 the translational axis and 150 Nm/rad in the rotational
473 axis, respectively. These values provided a reasonable
474 trade-off between the trajectory tracking performance
475 and the end-effector compliance. The human partner
476 was simultaneously provided with a visual feedback re-
477 garding the optimised configuration, which made sure
478 that the correct configuration was maintained.

479 4. Experimental Evaluation

480 Ten healthy male volunteers (age: 27.6 ± 2.3 years;
481 mass: 75.1 ± 5.3 kg; height: 1.80 ± 0.03 m)⁵ were re-
482 cruited for this study. The experiments were performed
483 at HRI² Lab of IIT, Italy. The study was approved by the
484 Regional Ethics Committee of Liguria (IIT_HRII.001,
485 108/2018).

486 First, we obtained the data for identification of dy-
487 namic model (i.e., SESC parameters) of each subject.
488 The subjects wore the MVN Biomech suit (Xsens Tech-
489 nologies BV) and stood on a Kistler force plate. They
490 were asked to perform 140 different static configura-
491 tions of their body. Note that the force plate is required
492 only during the off-line calibration and is not required
493 during the on-line phase.

494 The experimental setup is illustrated in Fig. 4. The
495 subjects wore the MVN Biomech suit to measure the
496 body configuration in real-time. The experimental eval-
497 uation involved a human-robot collaboration task. In
498 this scenario, the robot held an object that had to be pol-
499 ished by the human subject, who used a heavy hand-
500 held tool (mass: 3.4 kg). To do this, we developed a
501 simplified human body model with five joints (i.e., hip,
502 knee, ankle, shoulder and elbow), which primarily con-
503 tributed to Sagittal plane motion. Additionally, such a
504 model was interacting with environment using a single
505 hand and foot, hence, the contribution gain of hand and
506 foot were $\eta = 1$ and $\zeta = 1$, respectively. The task of the
507 robot was to bring the object to the human, while the
508 task of the human was to polish it⁶. In such a task, the

⁵Subject data is reported as: mean \pm standard deviation.

⁶This scenario can be generalised to other collaboration tasks (e.g., drilling, assembly, etc.) and handover tasks. For example, in the handover task the robot brings the object to the human, who then takes it from the robot at a certain position.

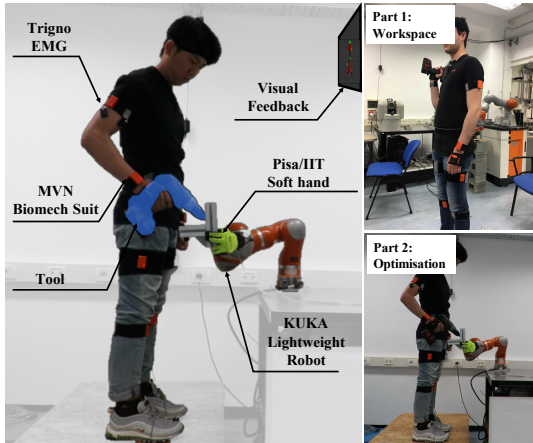


Figure 4: **Overview of the experimental setup.** The experimental setup consisted of a MVN Biomech suit, a KUKA LBR IV+ equipped with the Pisa/IIT soft hand, visual feedback and wireless EMG sensors. The experimental purpose consisted of two parts: task comparison in workspace of the arm, and evaluation in the optimisation.

robot should adapt its behaviour in a way that the working conditions are improved for the human co-worker, which signifies that any excessive joint load is prevented and the arm manipulability capacity value is maximised.

The whole-body configuration should ideally be in a pose where the overloading joint torques are as low as possible, while achieving a high arm manipulability capacity to facilitate an effective task execution. In the experiments, the arm manipulability capacity constraint was set to 80% of maximum capacity, which was obtained by scanning through the feasible arm workspace for each subject. This led to a good force and velocity production capacity in all directions since the human arm endpoint at the manipulation location had close-to-isotropic manipulability ellipsoid. The time required to scan through the feasible arm workspace for each subject was 87 seconds. However, this scanning process needs to be conducted only once for each subject and the result can be reused in future.

The experimental procedure was divided into two stages (as shown in the right of the Fig. 4). In the first stage, the subjects had to perform the given task in six different configurations of the arm, which were distributed around the workspace of the arm endpoint. See Fig. 5 for details and illustrations of the selected configurations. In the second stage, the proposed method was used to select the optimal working configuration in terms of overloading joint torques and given constraints (manipulability capacity, etc.). The on-line acquisition of the human body position data was performed using the MVN Biomech system. This data was then used to

calculate vector \mathbf{x}_0 and matrix \mathbf{B} that were necessary for real-time calculation of CoP in (2) and the human overloading joint torque vector in (8).

To compare the arm muscular effort during the task execution between the optimised configuration selected by the proposed method and the six different unoptimised configurations, we recorded and evaluated the muscle activity from electromyography (EMG) while performing the collaboration task. For the measurements, we selected Anterior Deltoid (AD), Posterior Deltoid (PD), Biceps Brachii (BB) and Triceps Brachii (TB), which are the dominant shoulder and elbow actuators in the given configurations. The EMG signals using Delsys Trigno Wireless system were first processed by rectification and low-pass filtering and were then normalised with respect to the maximal voluntary contraction to obtain the muscle activation for each muscle.

4.1. Results

The results of experiments are shown in Table 1, where we report the overloading joint torques, manipulability capacity value and muscle activity as measured by EMG. These variables were averaged across the subjects for each configuration. Fig. 6 shows summed mean values of overloading joint torques for different configurations. The mean manipulability capacity value for each configuration is presented in Fig. 7. The muscle activity capacity of the arm is shown in Fig. 8.

The configurations 1, 4 and 6 had overall lower overloading joint torque in the body than the optimised configuration. Statistical differences were tested with post-hoc t-tests with Bonferroni correction. The level of statistical significance used was .05 for all statistical tests. The difference was 21.73 ± 2.17^7 Nm ($p < .001$), 23.70 ± 2.19 Nm ($p < .001$) and 35.50 ± 1.48 Nm ($p < .001$), respectively. Even though the torque was lower in these configurations compared to the optimised configuration, the manipulability capacity was relatively low in all three compared to the optimised one. The difference was 55.31 ± 2.19 % ($p < .001$), 60.65 ± 5.59 % ($p < .001$) and 83.62 ± 2.10 % ($p < .001$), respectively. There were statistically significant differences in all values.

Configurations 2, 3, and 5 had higher joint torques compared to the optimised configuration. The differences were 33.82 ± 1.49 Nm ($p < .001$), 8.62 ± 1.68 Nm ($p < .001$) and 10.66 ± 1.21 Nm ($p < .001$), respectively. In addition, the manipulability capacity in these configurations was on average much lower. The difference

⁷The data is reported as: mean \pm standard error of mean.

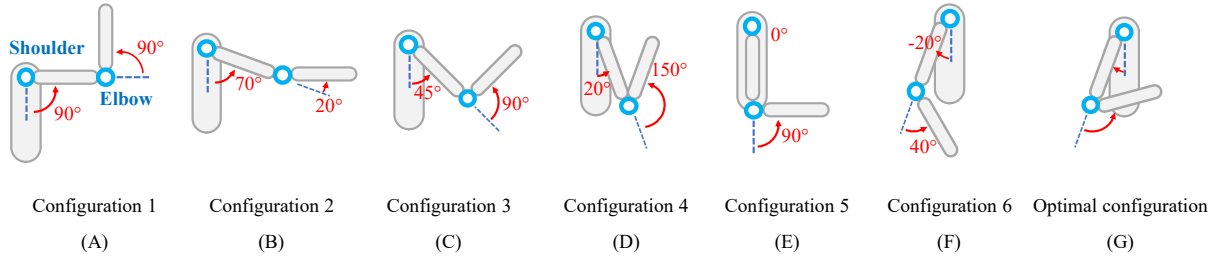


Figure 5: **The six different unoptimised configurations and the optimised configuration.** The optimal configuration was slightly different among the subjects, therefore the joint angle values were not specified.

Table 1: **Experimental results of ten subjects.** The results are separated according to seven different configurations. The data is reported as: mean (standard error of mean). Note that the optimal configuration was slightly different among the subjects.

Configuration		1 (Fig. 5A)	2 (Fig. 5B)	3 (Fig. 5C)	4 (Fig. 5D)	5 (Fig. 5E)	6 (Fig. 5F)	Optimal (Fig. 5G)
Manipulability capacity [%]		37.24 (1.46)	6.60 (1.00)	51.26 (5.76)	31.89 (5.20)	61.78 (3.29)	8.92 (0.79)	92.54 (1.19)
Overloading joint torque [Nm]	Hip	7.88 (0.67)	21.25 (0.60)	15.20 (0.550)	7.48 (0.69)	15.37 (0.46)	4.16 (0.35)	13.00 (0.46)
	Knee	8.57 (0.73)	21.67 (0.62)	15.72 (0.55)	8.03 (0.66)	15.89 (0.46)	4.73 (0.35)	13.35 (0.46)
	Ankle	9.57 (0.78)	22.52 (0.69)	16.61 (0.60)	8.93 (0.72)	16.71 (0.49)	5.56 (0.35)	14.15 (0.54)
	Shoulder	6.99 (0.30)	15.68 (0.25)	11.23 (0.17)	5.72 (0.28)	9.63 (0.20)	1.45 (0.26)	7.11 (0.26)
	Elbow	0.52 (0.13)	8.78 (0.14)	5.67 (0.15)	1.98 (0.31)	8.86 (0.14)	3.28 (0.22)	8.25 (0.17)
Muscle activity [%]	AD	42.61 (8.65)	80.97 (15.48)	48.25 (8.90)	13.92 (2.54)	10.46 (1.94)	4.95 (2.04)	3.59 (0.72)
	PD	18.19 (4.13)	50.54 (14.11)	10.87 (2.48)	2.98 (0.48)	2.85 (0.53)	21.49 (4.01)	7.65 (2.04)
	BB	2.28 (0.48)	18.06 (2.37)	8.44 (1.26)	15.10 (2.64)	13.87 (2.13)	5.38 (0.63)	15.60 (2.74)
	TB	16.75 (3.39)	27.88 (4.89)	10.01 (1.73)	17.35 (3.50)	10.46 (1.78)	7.86 (1.45)	19.09 (3.23)

588 was $85.94 \pm 2.17\%$ ($p < .001$), $41.28 \pm 4.77\%$ ($p < .001$) 601 $1.56 \pm 1.65\%$ ($p = .40$), respectively. The differences
589 and $30.76 \pm 2.77\%$ ($p < .001$), respectively. There were 602 were statistically insignificant.
590 statistically significant differences in all values.

591 The measured muscle activity capacity in the human 603
592 arm is shown in Fig. 8. The arm muscle activity in 604
593 configurations 1, 2 and 3 was relatively high in compar- 605
594 ison to the optimised configuration. The difference 606
595 was $8.47 \pm 2.74\%$ ($p = .017$), $32.88 \pm 7.25\%$ ($p = .0020$) 607
596 and $7.91 \pm 2.74\%$ ($p = .023$), respectively. The differ- 608
597 ences were statistically significant. On the other hand, 609
598 the muscle activity in configurations 4, 5 and 6 was 610
599 comparable to optimised configuration. The difference 611
600 was $0.85 \pm 1.39\%$ ($p = .58$), $2.07 \pm 1.21\%$ ($p = .14$) and

5. Discussion

From the results of overloading joint torques in different configurations, we can see that some of the tested configurations have overall lower torque in the body while performing the task. Even though the overall lower overloading joint torque would be more comfortable for the human worker, these configurations had significantly lower manipulability capacity of the arm, which could affect the task production. Since we spec-

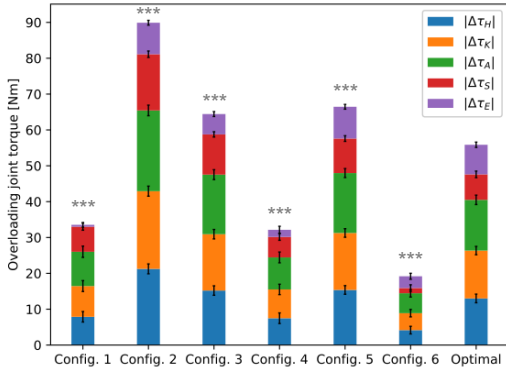


Figure 6: **The sum of all overloading joint torques for different configurations⁸.** Different colours in the bar represent different contribution from different joints.

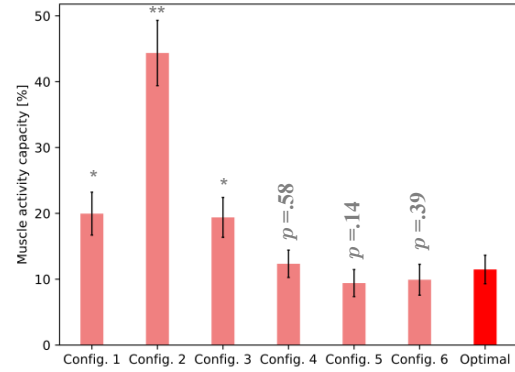


Figure 8: **The results⁸ of the muscle activity capacity of the arm for the different configurations.** The corresponded values are defined as a summation of subject-average muscle activations of all measured muscles, normalised by the number of muscles. This value represents the percentage of combined capacity of all four measured muscles.

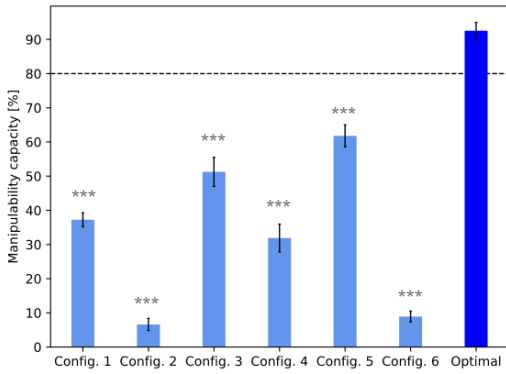


Figure 7: **The results⁸ of the manipulability capacity for different configurations.** The black dashed line denotes the manipulability capacity constraint set in the optimisation process.

612 ified a certain required degree of manipulability capac- 640
 613 ity in the optimisation process, the optimised configura- 641
 614 tion was constrained to the cases where the manipu- 642
 615 lability was above the prescribed threshold. If such 643
 616 high manipulability capacity is not required, the opti- 644
 617 misation could search within other configurations where 645
 618 overloading joint torques can be lower. The parameters 646
 619 of the proposed method, such as the required manipula- 647
 620 bility capacity, the constraints on configuration of body 648
 621 and the orientation of endpoint/tool, should therefore be 649
 622 selected based on the desired industrial task [15].

623 The results showed that there was considerably

624 higher combined arm muscle activity in configura-
 625 tions 1, 2 and 3 compared to that in configurations 4, 5, 6
 626 and the optimised configuration. The results also showed
 627 that the arm muscle activity in configurations 4, 5, 6
 628 and the optimised configuration was comparable, which
 629 indicates that the arm was approximately equally active
 630 in those configurations. Nevertheless, it should be noted
 631 that the muscle activity measurement was limited to the
 632 human arm, while optimisation of the overloading joint
 633 torques considered the whole body.

634 The main advantage of the proposed method is in
 635 its reduced complexity and limited amount of required
 636 measurement systems, which could significantly im-
 637 prove its applicability in real industrial environments.
 638 Further reduction of the complexity can be achieved by
 639 using more affordable motion capture systems (e.g., Mi-
 640 crosoft Kinect). However, some of the more affordable
 641 hardware might not be suitable for all kinds of industrial
 642 settings and tasks. The framework offers flexibility not
 643 only in terms of selecting the desired amount of DoF
 644 of human body, which is easily modifiable based on
 645 the desired complexity, but also adaptation to the kine-
 646 matic specifics of a task (e.g. changing tools, switching
 647 hands). Furthermore, task constraints can be modified
 648 based on the target task objectives, e.g., to impose con-
 649 straints on dual-arm manipulability, etc.

650 The manipulability could also be used as an objective
 651 rather than as a constraint. Using it as a constraint may
 652 lead to an absence of solution, however if the solution
 653 is found the manipulability is within the desired range.
 654 On the other hand, using it as an optimisation objective

⁸Asterisks indicate the level of statistical significance after post-hoc tests: * $p < .05$, ** $p < .01$ and *** $p < .001$

655 makes it less limiting on the number of possible solu- 705
656 tions, however it does not guarantee that the manipula- 706
657 bility will be in the desired range. This tradeoff should 707
658 be considered when selecting between the two options. 708
659

660 In the existing study we considered only manipula- 710
661 bility of the arm since in common industrial tasks, e.g. 711
662 using a machine to polish an object, the body is primar- 712
663 ily used to position the shoulder joint before the task is 713
664 performed and then it remain relatively static, while the 714
665 arm is doing majority of the movement required to per- 715
666 form the task. However, if the tasks require large move- 716
667 ments of the body, the proposed manipulability measure 717
668 can be extended to the body. 718
669

670 In the existing study we did not consider the elas- 720
671 tic properties of muscles, which have more dominant 721
672 role in explosive movements (e.g., jumping, throwing, 722
673 etc.), where the energy has to be transferred from prox- 723
674 imal muscles to distal muscles [45, 46]. The common 724
675 industrial tasks considered in this study do not involve 725
676 such explosive movements and therefore we considered 726
677 only antagonistic and configuration dependant nature of 727
678 joint torques produced by muscles in the musculoskele- 728
679 tal model. 729
680

681 The main goal of this paper was to introduce a 730
682 method that enables the robot to account for param- 731
683 eters related interaction dynamics during human-robot 732
684 collaboration and validate the approach on multiple sub- 733
685 jects. The future work will focus on determining to what 734
686 degree the considered parameters should be accounted 735
687 for and what would be the long term affects on human 736
688 subjects. 737
689

686 Funding

687 This work was supported in part by the H2020-ICT- 748
688 2019-2 project SOPHIA(GA 871237) and H2020-ICT 749
689 project ANDY (GA 731540). 750

690 References

- 691 [1] A. Ajoudani, A. M. Zanchettin, S. Ivaldi, A. Albu-Schäffer, 756
692 K. Kosuge, O. Khatib, Progress and prospects of the human- 757
693 robot collaboration, *Autonomous Robots* (2017). 758
- 694 [2] L. Peternel, N. Tsagarakis, A. Ajoudani, A human-robot co- 759
695 manipulation approach based on human sensorimotor informa- 760
696 tion, *IEEE Transactions on Neural Systems and Rehabilitation 761*
697 Engineering 25 (2017) 811–822. 762
- 698 [3] L. Peternel, N. Tsagarakis, D. Caldwell, A. Ajoudani, Robot 763
699 adaptation to human physical fatigue in human–robot co- 764
700 manipulation, *Autonomous Robots* 42 (2018) 1011–1021. 765
- 701 [4] A. De Luca, A. Albu-Schäffer, S. Haddadin, G. Hirzinger, Col- 766
702 lision detection and safe reaction with the DLR-III lightweight 767
703 manipulator arm, in: *Intelligent Robots and Systems (IROS), 768*
704 2006 IEEE/RSJ Intl. Conf. on, pp. 1623–1630. 769

- [5] D. Kulić, E. Croft, Pre-collision safety strategies for human- 705
robot interaction, *Autonomous Robots* 22 (2007) 149–164. 706
- [6] V. Magnanimo, S. Walther, L. Tecchia, C. Natale, T. Guhl, Safe- 707
guarding a mobile manipulator using dynamic safety fields, in: 708
Intelligent Robots and Systems (IROS), 2016 IEEE/RSJ Inter- 709
national Conference on, IEEE, pp. 2972–2977. 710
- [7] A. Albu-Schäffer, C. Ott, G. Hirzinger, A unified passivity- 711
based control framework for position, torque and impedance 712
control of flexible joint robots, *Int. J. Rob. Res.* 26 (2007) 23– 713
39. 714
- [8] S. Haddadin, S. Haddadin, A. Khoury, T. Rokahr, S. Parusel, 715
R. Burgkart, A. Bicchi, A. Albu-Schäffer, On making robots 716
understand safety: Embedding injury knowledge into control, 717
The International Journal of Robotics Research 31 (2012) 1578– 718
1602. 719
- [9] J. Kim, A. Alspach, K. Yamane, 3d printed soft skin for safe 720
human-robot interaction, in: *Intelligent Robots and Systems 721*
(IROS), 2015 IEEE/RSJ Int. Conf. on, IEEE, pp. 2419–2425. 722
- [10] N. Mansfeld, M. Hamad, M. Becker, A. G. Marin, S. Had- 723
dadin, Safety map: A unified representation for biomechanics 724
impact data and robot instantaneous dynamic properties, *IEEE 725*
Robotics and Automation Letters 3 (2018) 1880–1887. 726
- [11] P. Evrard, E. Gribovskaya, S. Calinon, A. Billard, A. Khed- 727
dar, Teaching physical collaborative tasks: object-lifting case 728
study with a humanoid, in: *IEEE-RAS Intl. Conf. on Humanoid 729*
Robots, pp. 399–404. 730
- [12] L. Peternel, T. Petrič, E. Oztop, J. Babič, Teaching robots to 731
cooperate with humans in dynamic manipulation tasks based on 732
multi-modal human-in-the-loop approach, *Autonomous robots 733*
36 (2014) 123–136. 734
- [13] H. Ben Amor, G. Neumann, S. Kamthe, O. Kroemer, J. Peters, 735
Interaction primitives for human-robot cooperation tasks, in: 736
Robotics and Automation (ICRA), 2014 IEEE Intl. Conf. on, 737
pp. 2831–2837. 738
- [14] W. M. Keyserling, D. B. Chaffin, Occupational ergonomics- 739
methods to evaluate physical stress on the job, *Annual review 740*
of public health 7 (1986) 77–104. 741
- [15] S. E. Mathiassen, T. Möller, M. Forsman, Variability in me- 742
chanical exposure within and between individuals performing a 743
highly constrained industrial work task, *Ergonomics* 46 (2003) 744
800–824. 745
- [16] S. Kumar, Theories of musculoskeletal injury causation, *Er- 746*
gonomics 44 (2001) 17–47. 747
- [17] G. B. Andersson, Epidemiologic aspects on low-back pain in 748
industry., *Spine* 6 (1981) 53–60. 749
- [18] S. L. Sauter, L. R. Murphy, J. J. Hurrell, Prevention of work- 750
related psychological disorders: A national strategy proposed by 751
the national institute for occupational safety and health (niosh)., 752
American Psychologist 45 (1990) 1146. 753
- [19] M. Peruzzini, M. Pellicciari, M. Gadaleta, A comparative study 754
on computer-integrated set-ups to design human-centred manu- 755
facturing systems, *Robotics and Computer-Integrated Manu- 756*
facturing 55 (2019) 265–278. 757
- [20] M. Millard, T. Uchida, A. Seth, S. L. Delp, Flexing compu- 758
tational muscle: modeling and simulation of musculotendon 759
dynamics, *Journal of biomechanical engineering* 135 (2013) 760
021005. 761
- [21] J. Jovic, A. Escande, K. Ayusawa, E. Yoshida, A. Kheddar, 762
G. Venture, Humanoid and human inertia parameter identifi- 763
cation using hierarchical optimization, *IEEE Transactions on 764*
Robotics 32 (2016) 726–735. 765
- [22] S. Gallagher, W. S. Marras, K. G. Davis, K. Kovacs, Effects 766
of posture on dynamic back loading during a cable lifting task, 767
Ergonomics 45 (2002) 380–398. 768
- [23] J. C. E. Van Der Burg, J. H. Van Dieën, H. M. Toussaint, Lifting 769

- an unexpectedly heavy object: The effects on low-back loading and balance loss, *Clinical Biomechanics* 15 (2000) 469–477.
- [24] E. A. Sisbot, L. F. Marin-Urias, R. Alami, T. Simeon, A human aware mobile robot motion planner, *IEEE Transactions on Robotics* 23 (2007) 874–883.
- [25] K. Strabala, M. K. Lee, A. Dragan, J. Forlizzi, S. Srinivasa, M. Cakmak, V. Micelli, Towards seamless human-robot handovers, *Journal of Human-Robot Interaction* 1 (2013).
- [26] A. M. Bestick, S. A. Burden, G. Willits, N. Naikal, S. S. Sastry, R. Bajcsy, Personalized kinematics for human-robot collaborative manipulation, in: *Intelligent Robots and Systems (IROS), 2015 IEEE/RSJ International Conference on*, IEEE, pp. 1037–1044.
- [27] B. Navarro, A. Cherubini, A. Fonte, G. Poisson, P. Fraise, A Framework for intuitive collaboration with a mobile manipulator, in: *Intelligent Robots and Systems (IROS), 2015 IEEE/RSJ Intl. Conf. on*, pp. 1–8.
- [28] N. Vahrenkamp, H. Arnst, M. Wchter, D. Schiebener, P. Sotiropoulos, M. Kowalik, T. Asfour, Workspace analysis for planning human-robot interaction tasks, in: *2016 IEEE-RAS 16th International Conference on Humanoid Robots (Humanoids)*, pp. 1298–1303.
- [29] L. Peternel, C. Fang, N. Tsagarakis, A. Ajoudani, A selective muscle fatigue management approach to ergonomic human-robot co-manipulation, *Robotics and Computer-Integrated Manufacturing* 58 (2019) 69–79.
- [30] W. Kim, J. Lee, N. Tsagarakis, A. Ajoudani, A real-time and reduced-complexity approach to the detection and monitoring of static joint overloading in humans, in: *Rehabilitation Robotics (ICORR), 2017 International Conference on*, IEEE, pp. 828–834.
- [31] W. Kim, J. Lee, L. Peternel, N. Tsagarakis, A. Ajoudani, Anticipatory robot assistance for the prevention of human static joint overloading in human-robot collaboration, *IEEE Robotics and Automation Letters* 3 (2018) 68–75.
- [32] P. Maurice, P. Schlehuber, V. Padois, Y. Measson, P. Bidaud, Automatic selection of ergonomic indicators for the design of collaborative robots: A virtual-human in the loop approach, in: *2014 IEEE-RAS International Conference on Humanoid Robots*, pp. 801–808.
- [33] P. Maurice, V. Padois, Y. Measson, P. Bidaud, Experimental assessment of the quality of ergonomic indicators for dynamic systems computed using a digital human model, *International Journal of Human Factors Modelling and Simulation* 5 (2016) 190–209.
- [34] L. Peternel, W. Kim, J. Babič, A. Ajoudani, Towards ergonomic control of human-robot co-manipulation and handover, in: *2017 IEEE-RAS 17th International Conference on Humanoid Robotics (Humanoids)*, pp. 55–60.
- [35] D. A. Winter, Human balance and posture control during standing and walking, *Gait & posture* 3 (1995) 193–214.
- [36] M. B. Popovic, A. Goswami, H. Herr, Ground reference points in legged locomotion: Definitions, biological trajectories and control implications, *The International Journal of Robotics Research* 24 (2005) 1013–1032.
- [37] A. González, M. Hayashibe, V. Bonnet, P. Fraise, Whole body center of mass estimation with portable sensors: Using the statically equivalent serial chain and a kinect, *Sensors* 14 (2014) 16955–16971.
- [38] P. R. Bélanger, P. Dobrovolny, A. Helmy, X. Zhang, Estimation of angular velocity and acceleration from shaft-encoder measurements, *The International Journal of Robotics Research* 17 (1998) 1225–1233.
- [39] M. Lorenzini, W. Kim, E. De Momi, A. Ajoudani, A synergistic approach to the real-time estimation of the feet ground reaction forces and centers of pressure in humans with application to human-robot collaboration, *IEEE Robotics and Automation Letters* 3 (2018) 3654–3661.
- [40] S. H. Snook, V. M. Ciriello, The design of manual handling tasks: revised tables of maximum acceptable weights and forces, *Ergonomics* 34 (1991) 1197–1213.
- [41] E. Rueckert, J. Čamernik, J. Peters, J. Babič, Probabilistic Movement Models Show that Postural Control Precedes and Predicts Volitional Motor Control., *Scientific reports* 6 (2016) 28455.
- [42] T. Yoshikawa, Manipulability of Robotic Mechanisms, *The Intl. Journal of Robotics Research* 4 (1985) 3–9.
- [43] K. Ohta, Y. Tanaka, I. Kawate, T. Tsuji, Human muscular mobility ellipsoid: End-point acceleration manipulability measure in fast motion of human upper arm, *Journal of Biomechanical Science and Engineering* 9 (2014) 14–00207.
- [44] R. Goljat, J. Babič, T. Petrič, L. Peternel, J. Morimoto, Power-augmentation control approach for arm exoskeleton based on human muscular manipulability, in: *Robotics and Automation (ICRA), 2017 IEEE Intl. Conf. on*, pp. 5929–5934.
- [45] K. Kubo, Y. Kawakami, T. Fukunaga, Influence of elastic properties of tendon structures on jump performance in humans, *Journal of applied physiology* 87 (1999) 2090–2096.
- [46] N. T. Roach, M. Venkadesan, M. J. Rainbow, D. E. Lieberman, Elastic energy storage in the shoulder and the evolution of high-speed throwing in homo, *Nature* 498 (2013) 483.